RSC Advances

PAPER

View Article Online
View Journal | View Issue

Cite this: *RSC Adv.*, 2018, **8**, 35306

Core–shell structured $NaYF_4$:Yb,Tm@CdS composite for enhanced photocatalytic properties

Pengpeng Feng, Yusong Pan * and Hui Ye

Received 13th August 2018
Accepted 8th October 2018

DOI: 10.1039/c8ra06800c

rsc.li/rsc-advances

$NaYF_4$:Yb,Tm upconversion nanocrystals with hexagonal structure possess excellent photoluminescence emission characteristics. Under near infrared (NIR) light irradiation, the Yb^{3+} ions act as sensitizers to absorb the NIR light and transform NIR light into ultraviolet (UV) and visible (Vis) light continuously. Hybrid NIR-activated photocatalysts can be fabricated by combining upconversion nanocrystals with various semiconductor nanocrystals. In this paper, $NaYF_4$:Yb,Tm micro-rods were hydrothermally synthesized with oleic acid as capping ligand. The $NaYF_4$:Yb,Tm@CdS composite was fabricated by *in situ* generation of CdS nanoclusters on the surface of $NaYF_4$:Yb,Tm micro-rods. The morphologies and structures of NaY_4:Yb,Tm and $NaYF_4$:Yb,Tm@CdS were characterized by XRD, SEM, TEM, XPS, UV-Vis and PL spectroscopy. The results of photocatalytic experiments indicated that the $NaYF_4$:Yb,Tm@CdS composite displayed photocatalytic activity under NIR irradiation. In comparison with pure CdS, the photocatalytic ability of $NaYF_4$:Yb,Tm@CdS composite under Vis-NIR irradiation was obviously enhanced. 82% of RhB was degraded by $NaYF_4$:Yb,Tm@CdS catalyst within 75 min under Vis-NIR irradiation, which was more effective than pure CdS (65% degradation of RhB).

1 Introduction

Recently, environmental pollution has become an urgent problem to be solved worldwide. It is well known that photocatalytic techniques are widely applied to solve the issue of water pollution because they are environmentally friendly.[1–4] Among various photo-catalysts, nano-structured cadmium sulfide (CdS) is one of the most widely studied and used photocatalysts because of its narrow band gap (~2.42 eV) at room temperature.[5,6] In order to improve photocatalytic efficiency, many methods have been applied including the adjustment of particle size, morphology and surface area of the photocatalyst.[7–9] Furthermore, many technologies, such as deposition of noble metals or non-metals, doping of noble metals or non-metals and coupling with other semiconductors, have been used to improve the utilization of visible light by CdS.[10–13] However, near-infrared light that accounts for about 45% of solar energy was not fully utilized by photocatalysts in those efforts.[14]

To address the above problems, upconversion (UC) nanocrystals can be used as light transmitter. It is recognized as one of the promising methods to improve the utilization of sunlight by combining them with matching semiconductors.[15–17] Recently, the β-$NaYF_4$:25 wt% Yb^{3+}, 0.6 wt% Tm^{3+}@TiO_2 composites were synthesized by the hydrolysis of TTIP, which decomposes about 69% of MO (76% of RhB and 68% of MB) within 24 h under simulated 980 nm laser irradiation.[18] Shi *et al.* synthesized the β-NaYF4:Yb^{3+},Tm^{3+}@SiO_2@TiO_2 core–shell nanocrystals by the micro-emulsion method. The results of photocatalytic experiment showed that more than 76% MO were degraded within 60 min under the simulated solar light irradiation with the existence of $NaYF_4$:Yb^{3+},Tm^{3+}@SiO_2@TiO_2 nano-composites. In contrast, only 7% MO were decomposed in the presence of the same amount of TiO_2.[19] Guo *et al.* reported that β-NaYF4:Yb^{3+},Tm^{3+}@ZnO nano-composites were synthesized *via* a two-step high temperature thermolysis method. The photocatalyst of β-NaYF4:Yb^{3+},Tm^{3+}@ZnO resulted in 65% degradation of RhB within 30 h under simulated 980 nm laser irradiation.[20] Tou *et al.* prepared β-$NaYF_4$:Yb,Tm@amorphous SiO_2@wurtzite ZnO core–shell–shell nanoparticles. The nanoparticles showed good photocatalytic activity under the 980 nm laser irradiation and decomposed about 87% RhB within 100 min under the simulated sunlight irradiation.[21] However, $NaYF_4$:Yb^{3+},Tm^{3+} nanoparticles show low UV emissions and relatively strong visible light emissions. Unfortunately, the visible light in those emissions cannot be harnessed by the ZnO and TiO_2 shells. In order to improve utilization of visible light emissions, Yu *et al.* reported the combination of $NaYF_4$:Yb^{3+},Tm^{3+} with a narrower band-gap CdS. However, the process of $NaYF_4$:Yb^{3+},Tm^{3+}/CdS composites reported by Yu *et al.* is complex, which includes the individual preparation of functional $NaYF_4$:Yb,Tm and CdS particles, and then linking them through $SHCH_2COOH$ and $SHCH_2CH_2OH$ chains. Moreover, the synthetic $NaYF_4$:Yb^{3+},Tm^{3+} showed low upconversion fluorescence properties.[22]

School of Material Science & Engineering, Anhui University of Science and Technology, Huainan, China 232001. E-mail: yusongpan@163.com

In the present work, a new composite consisting of $NaYF_4$:Yb^{3+},Tm^{3+} and narrower band-gap CdS nanoparticle was fabricated through a two-step hydrothermal method. The photocatalytic properties of the core–shell structured $NaYF_4$:Yb,Tm@CdS composite were investigated by photo-degradation of RhB under the irradiation of NIR and Vis-NIR light. The developed composites may have prospective applications in the environmental remedy.

2 Experimental

2.1 Materials

Rare earth oxide (Y_2O_3, Yb_2O_3, Tm_2O_3, 99.99 wt%) were all purchased from Shang Macklin Biochemical Co. Ltd., China. Sodium hydroxide (NaOH, 98 wt%), ammonium fluoride (NH_4F, 98 wt%), oleic acid (OA, 90%), trisodium citrate dihydrate ($C_6H_5Na_3O_7 \cdot 2H_2O$, 98 wt%), ammonia aqueous solution ($NH_3 \cdot H_2O$, 25–28% wt%), cadmium chloride ($CdCl_2$, 99 wt%), and ethanol (99.7 wt%) were purchased from Aladdin Industrial Corporation, China. Hydrochloric acid (HCl, 36–38 wt%) was supplied by Wu Xi City Yasheng Chemical Co. Ltd., China. Thioacetamide (TAA, 99.0 wt%) was purchased from Sinopharm Chemical Reagent Co. Ltd., China. All raw materials were used as starting materials without further purification.

2.2 Synthesis of water-dispersible $NaYF_4$:Yb,Tm microrods

The $NaYF_4$:30%Yb, 0.5%Tm microrods was synthesized according to the previous method.[23] The detailed synthesis process was described as follows. Firstly, Y_2O_3 (0.7 mmol), Yb_2O_3 (0.3 mmol), Tm_2O_3 (0.005 mmol) were fully dissolved in the hydrochloric acid, and then the solution was heated to evaporate water completely to obtain rare earth chlorides. Secondly, a 7.5 ml deionized water solution of 1.5 g NaOH was mixed with 25 ml ethanol and 25 ml oleic acid under stirring. Thirdly, the as-prepared rare earth chlorides were dissolved in 10 ml deionized water to obtain mixture solution of rare earth chlorides. Then, the 10 ml as-prepared rare earth chlorides mixture solution was added to the above mixture solution and stirred continuously for 30 min, followed by adding 5 ml of NH_4F (2 M) into the flask and continuous stirring for another 60 min. Finally, the liquid mixture was poured into the Teflon-lined autoclave, which was sealed and maintained at 220 °C for 12 h. After the autoclave was cooled to room temperature, the obtained product was collected by centrifugation, and washed with distilled water and absolute ethanol three times.

The water-dispersible $NaYF_4$:Yb,Tm microrods were prepared by protonation method.[24] Typically, 1 mmol $NaYF_4$:Yb,Tm was added into 20 ml deionized water, the pH value of the $NaYF_4$:Yb,Tm solution was adjusted to 4 by slow dropping diluted HCl (0.1 M) under magnetic stirring. This process was maintained for 2 h at room temperature. Then 10 ml of hexane was mixed with the solution and the water-dispersible $NaYF_4$:Yb,Tm was collected by centrifugation, washed with ethanol and deionized water three times and finally added to 10 ml aqueous solution.

2.3 Synthesis of $NaYF_4$:Yb,Tm@CdS core–shell composites

Typically, 0.06 g $NaYF_4$:Yb,Tm was dispersed in 140 ml deionized water by sonication treatment for 30 min. Trisodium citrate dihydrate (7 mL, 0.1 M) and $CdCl_2$ (7 mL, 0.08 M) were sequentially added to the above solution under continuous stirring for 20 min and 40 min, respectively. After then, ammonia aqueous solution was slowly dropped in the mixture solution until the pH value reached 10.5. Subsequently, the mixture solution was slowly heated to 65 °C in a bath. Then, 10 ml TAA (0.063 M) was slowly injected into the above solution with 0.1 ml min^{-1} by the peristaltic pump. The reaction was kept for another 1 h at 65 °C. The final product was washed with ethanol and deionized water for several times, and dried at 60 °C for 12 h in an oven.

2.4 Characterizations

Powder X-ray diffraction (XRD) was carried out on a Bruker D8 ADVANCE X-ray diffractometer equipped with Cu K_α radiation (λ = 0.15418 nm). The SEM images was obtained using FEI QUANTA 400. High Resolution Transmission electron microscopy (HRTEM) was performed on a FEI Tecnai G2 F20 electron microscope at an accelerating voltage of 200 kV. The HRTEM samples were prepared by dropping a suspension of $NaYF_4$:Yb,Tm@CdS composites on a carbon-film coated copper grid. UV-Vis absorption spectra were obtained under the diffuse reflection mode using a METASH UV-9000S spectrometer with $BaSO_4$ as the reference sample. The surface chemical environments were analyzed by X-ray photoelectron spectra (XPS) using an ESCALAB 250 Xi spectrometer with monochromatic Al K_α X-rays at 150 W. The photoluminescence spectra of photocatalysts were tested on the Edinburgh Instruments FS5 fluorescence spectrometer with a 980 nm laser as the excitation source.

2.5 Photocatalytic experiments

The photocatalytic performances of the CdS and $NaYF_4$:Yb,Tm @CdS composites were evaluated by the degradation of RhB solution under irradiation of a 300 W xenon lamp (PLS-SXE300). Visible band-pass (400–800 nm) and NIR band-pass (800–2500 nm) were obtained through choosing the suitable light filters. For each experiment, 10 mg photocatalyst was mixed with 50 ml RhB (2×10^{-5} M). Before illumination, the suspensions were magnetically stirred in dark for 1 h to reach adsorption–desorption equilibrium. During the process of light irradiation, aliquots of about 4 ml were withdrawn at given time intervals and centrifuged to remove the photocatalyst particles and then was tested the concentration of RhB by UV-Vis spectroscopy at 554 nm.

3 Results and discussion

3.1 SEM and TEM images

Fig. 1 shows the typical SEM images of the as-synthesized $NaYF_4$:Yb,Tm micro-rods. These micro-rods are uniform in size and exhibit a hexagonal rod-like shape with a diameter of *ca.* 240–270 nm (diagonal length) and a length of *ca.* 1.4–1.7 μm. Careful observation from Fig. 1, the single micro-rod of

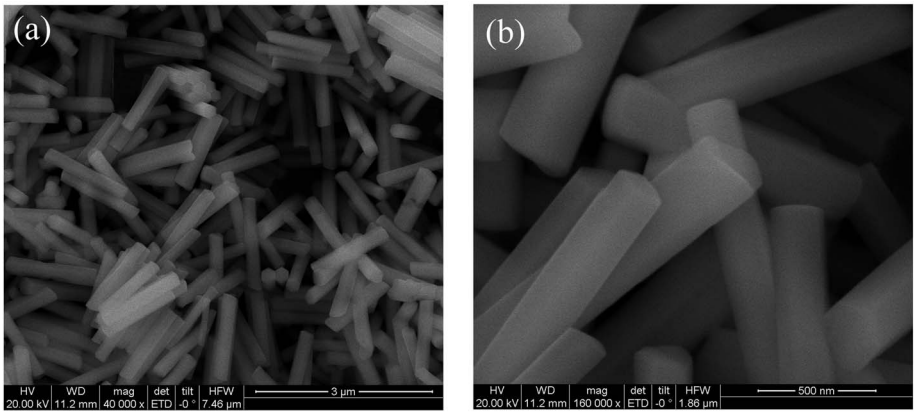

Fig. 1 SEM images of as-prepared $NaYF_4$:Yb,Tm microrods at different magnifications (a) ×40k and (b) ×160k.

$NaYF_4$:Yb,Tm presents a clear and smooth surface. In order to efficiently deposit CdS particles on the surface of $NaYF_4$:Yb,Tm micro-rod, the hydrophobic ligand of oleic acid on the surface of $NaYF_4$:Yb,Tm micro-rod was removed by washing with diluted hydrochloric acid. After removing of hydrophobic ligand, the wettability of $NaYF_4$:Yb,Tm changed from hydrophobic to hydrophilic.

Fig. 2 shows the morphologies of the prepared $NaYF_4$:Yb,Tm@CdS samples were characterized by HRTEM. HRTEM images of $NaYF_4$:Yb,Tm@CdS composite give a better insight into their structural information. As shown in Fig. 2a and b, one can observe the obvious deposition of CdS particles on the surface of $NaYF_4$:Yb,Tm micro-rod and formation of core–shell structure. The black cores are the $NaYF_4$:Yb,Tm micro-rods. The grayish white spots around the surface of micro-rods should be CdS particles and formation the shell of the composite. The thickness of the CdS shell is about 22–25 nm. The lattice distance of 0.1753 nm matches well with the *d* spacing of (311) planes of the cubic CdS crystal (See Fig. 2c). Furthermore, it can be clearly observed that the CdS particles exist in the form of nano-clusters. One single nano-cluster possesses microporous-like structure which formed by many tiny CdS particles. Comparison with compact CdS shell, the nano-clusters of CdS shell with microporous-like structure may provide two advantages. On the one hand, the microporous-like structure of nano-clusters is beneficial for the catalyst adsorption of the reactant. Sufficient adsorption of reactants is a crucial step for the whole photocatalytic process and it is also a key parameter to determine the overall efficiency of the photocatalyst. On the other hand, the microporous-like structure of CdS shell may allow more NIR light to reach the $NaYF_4$:Yb,Tm core due to the reduced shielding effect of the microporous CdS shell.

Currently, upconversion materials preparation technologies mainly include hydrothermal and solvothermal methods. In solvothermal method, the mixture of oleic acid/octadecene or oleic acid/oleylamine is usually used as a solvent. The function of oleic acid not only plays the role of capping ligand but also controls the crystal growth. $NaYF_4$:Yb,Tm upconversion materials prepared by solvothermal method have the characteristics of nanometer particle in size and regular morphology. In hydrothermal method, the deionized water is used as a solvent, and organic polymers such as PVP, CTAB and SDS are used as templates.[25,26] Hydrothermal method is conducive to the synthesis of upconversion materials with larger particle size, but the morphology is generally difficult to be controlled. It should be noted that the light conversion capability of upconversion materials is closely to the size of the materials. The larger the particle size, the stronger the light conversion capability of the material.[27]

In our work, we successfully hydrothermally synthesized the $NaYF_4$:Yb,Tm micro-rod with regular hexagonal structure using oleic acid as capping ligand. The size of $NaYF_4$:Yb,Tm micro-rod with hexagonal structure is on the micro-scale in the length direction and on the nano-scale in the diameter direction. Such

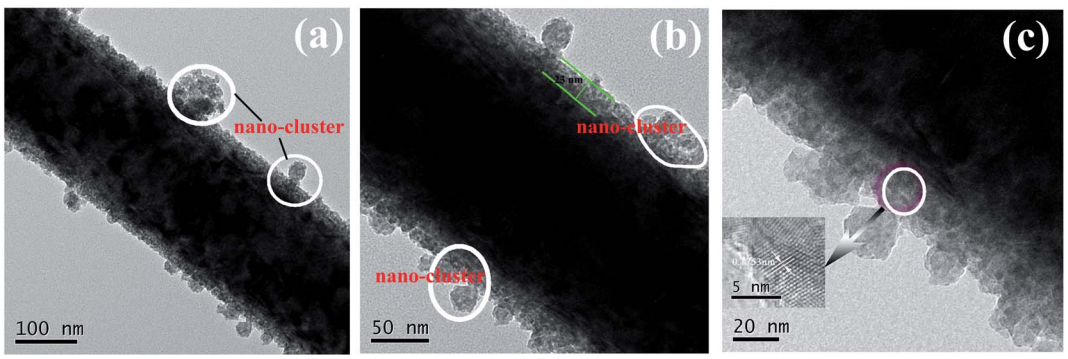

Fig. 2 TEM images of prepared $NaYF_4$:Yb,Tm@CdS at different magnifications (a) scale bar, 100 nm, (b) scale bar, 50 nm and (c) scale bar, 20 nm.

micro- and nano-scale structures of $NaYF_4$:Yb,Tm hexagonal micro-rod can effectively improve the specific surface area and light conversion capability, and ultimately enhancing the photocatalytic degradation of organic reactant.

3.2 XRD and XPS analysis

Fig. 3 shows the XRD patterns of $NaYF_4$:Yb,Tm, CdS, and $NaYF_4$:Yb,Tm@CdS, respectively. As shown in Fig. 3a, all characteristic peaks from the sample can be matched well with that of pure β-$NaYF_4$:Yb,Tm crystal (JCPDS no. 16-0334). No peaks from cubic-phase crystals or impurities are found, suggesting the sample is hexagonal phase with highly crystallization. After deposition of CdS on the surface of $NaYF_4$:Yb,Tm to form core–shell structure, two sets of diffraction peaks were found in the XRD patterns of $NaYF_4$:Yb,Tm@CdS composite (see Fig. 3b). One set of peaks is consistent with the β-$NaYF_4$:Yb,Tm crystals (hexagonal structure), while the other set of peaks matches finely with cubic CdS crystals (JCPDS no. 10-0454) (see Fig. 3c). However, it can be found from Fig. 3b that the diffraction peaks of CdS obviously widened, suggesting the crystal grain of CdS particles refining. In order to estimate the size of CdS crystal grain, the CdS particles were prepared with same experimental parameters in the absence of $NaYF_4$:Yb,Tm. The XRD pattern of pure CdS is shown in Fig. 3c. The diffraction peaks in Fig. 3c is accordance with the cubic CdS crystal (JCPDS no. 10-0454). It is interesting found that all the diffraction peaks of CdS crystal grain widened, suggesting the size of crystal grain of CdS is on the nano-scale. The average size of CdS crystal grain is 3–5 nm calculated by Scherrer equation. This result is consistent with the observation result of HRTEM image.

To further prove the chemical composition of the as-synthesized photocatalyst, the XPS of $NaYF_4$:Yb,Tm@CdS in which the elements of Cd, S, Na, Y, Yb, Tm, and F were given in Fig. 4. Two binding energy peaks representing at 405.1 eV and 411.7 eV in Fig. 4b corresponded to the core levels of Cd $3d_{3/2}$ and Cd $3d_{5/2}$, respectively. The core levels of S $2p_{1/2}$ and S $2p_{3/2}$ are located at 161.6 eV and 163.6 eV in Fig. 4c. These results were in accordance with the reported core levels of the CdS nanoparticles.[6,28] XPS peaks of Na (1s, 1072.2 eV), Y ($3d_{3/2}$, 159.3 eV), Y ($3d_{5/2}$, 161.6 eV), F (1s, 185.52 eV) were also found in Fig. 4d–f.[29–31]

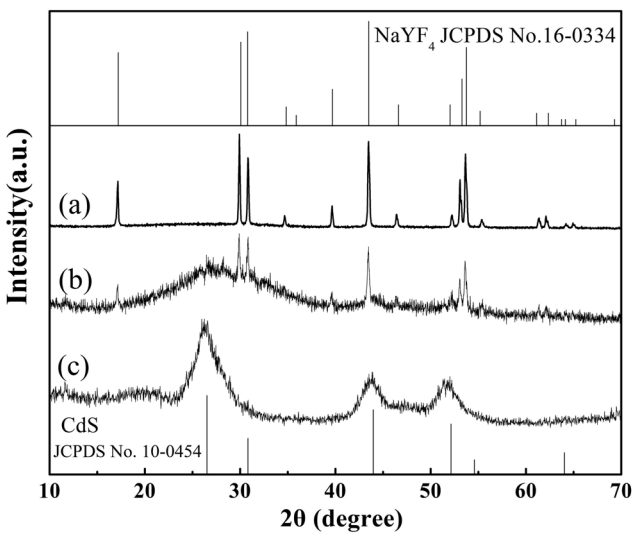

Fig. 3 XRD patterns of (a) $NaYF_4$:Yb,Tm, $NaYF_4$:Yb, (b) Tm@CdS, and (c) CdS. Standard XRD patterns of $NaYF_4$:Yb,Tm and CdS are given as references.

3.3 Optical properties

The UV-Vis diffuse reflectance spectra of the CdS, $NaYF_4$:Yb,Tm@CdS and $NaYF_4$:Yb,Tm are displayed in Fig. 5a, respectively. UV-Vis diffuse reflectance spectra shows that the pure $NaYF_4$:Yb,Tm do not display evident absorption in the UV-Vis region and the pure CdS shows obvious absorption in the UV-Vis region. However, the as-synthesized $NaYF_4$:Yb,Tm@CdS shows a strong absorption in the UV-Vis region. Furthermore, it can be concluded from Fig. 5a that the CdS has a narrow band gap of 1.97 eV (absorption edge at 628 nm), while the band gap of $NaYF_4$:Yb,Tm@CdS is about 2.03 eV (absorption edge at 610 nm).

It is well known that $NaYF_4$ particle is an excellent host-matrix for upconversion luminescence when co-doped Yb^{3+} and Tm^{3+} in the $NaYF_4$. The $NaYF_4$:Yb,Tm would produce strong upconversion emissions under 980 nm NIR excitation. Yb^{3+} plays the role of sensitizer ion for continuous absorption of 980 nm NIR light and Tm^{3+} acts as an activator ion to emit of a series of spectra with wavelengths less than 980 nm. Fig. 5b shows the upconversion photoluminescence spectra of $NaYF_4$:Yb,Tm and $NaYF_4$:Yb,Tm@CdS under 980 nm wavelength excitation, respectively. A series of spectral peaks appears for $NaYF_4$:Yb,Tm under 980 nm wavelength excitation. Three strong peaks located at 290, 347 and 362 nm, which derived from the radioactive transitions of $^1I_6 \rightarrow {}^3H_6$, $^1I_6 \rightarrow {}^3F_4$ and $^1D_2 \rightarrow {}^3H_6$. The other two peaks at 452 and 476 nm can be assigned to the transitions of the $^1D_2 \rightarrow {}^3F_4$ and $^1G_4 \rightarrow {}^3H_6$ of Tm^{3+} ion. However, it is found that all these upconversion peaks weaken evidently after deposited with CdS. The remarkable decrease in upconversion emissions is mainly ascribed to two factors. On the one hand, the existence of CdS shell has a scattering and shielding effects on the incident NIR light. On the other hand, the decrease in upconversion emissions would be attributed to the absorption of the CdS nanocluster shell. Just as shown in Fig. 5a, CdS can effectively absorb light with wavelength lower than 628 nm, but hardly absorbs light with wavelength higher than 628 nm. Thus, the peak intensities in the lower light wavelengths (250 nm to 620 nm) of $NaYF_4$:Yb,Tm@CdS are lower to that of $NaYF_4$:Yb,Tm due to the absorption of the CdS shell. The peak intensities in the higher light wavelengths (>620 nm) are quite similar for the two samples since CdS shell can hardly absorbs light waves with wavelength higher than 620 nm.

3.4 Photocatalytic study

Photodegradation of the $NaYF_4$:Yb,Tm@CdS composite was evaluated by using RhB as model pollutant. For the purpose of comparison, both naked $NaYF_4$:Yb,Tm and CdS are employed as references. Fig. 6a and c displays the UV-Vis absorption spectra of the RhB solution photo-catalyzed by

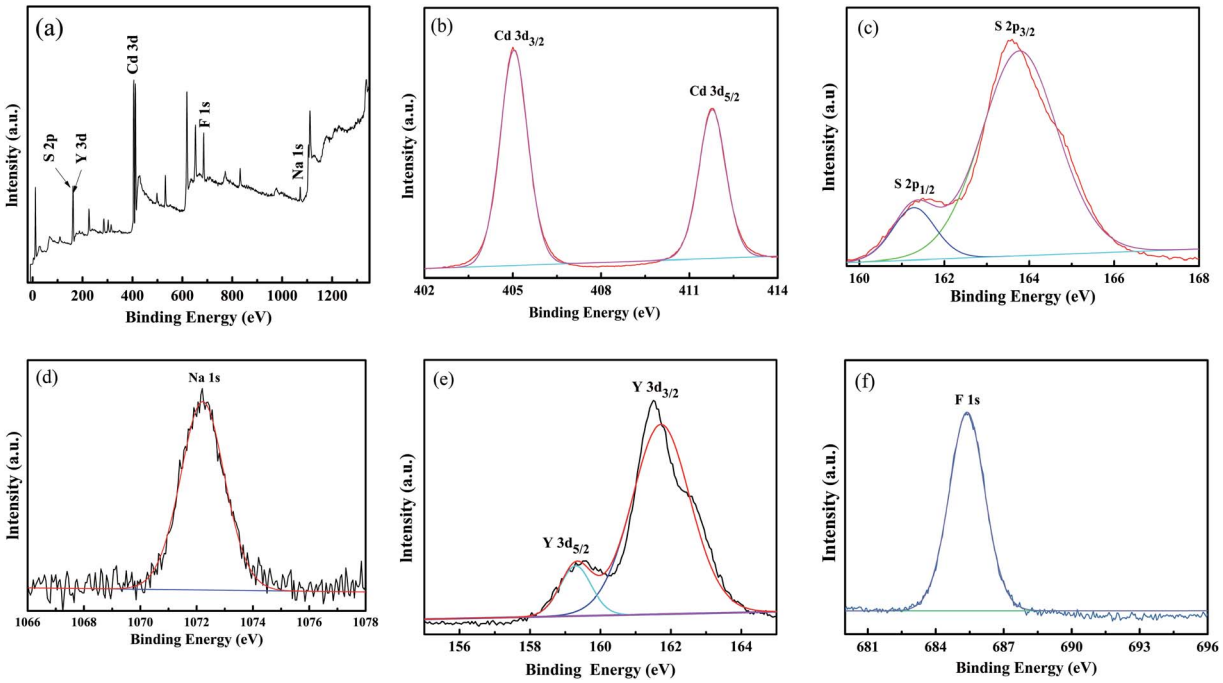

Fig. 4 (a) XPS spectra survey of $NaYF_4$:Yb^{3+},Tm^{3+}@CdS composites; (b) XPS spectra of Cd element; (c) XPS spectra of S element; (d) XPS spectra of Na element; (e) XPS spectra of Y element; (f) XPS spectra of F element.

$NaYF_4$:Yb,Tm@CdS composite for different irradiation time under NIR (800–2500 nm) and Vis-NIR (400–2500 nm) irradiation, respectively. It can be found that the concentration of RhB solution gradually decreases under irradiation of the NIR light (see Fig. 6a). This result verified that the $NaYF_4$:Yb,Tm@CdS has perceivable photocatalytic activity even under NIR irradiation. Considering that both the naked $NaYF_4$:Yb,Tm and CdS have almost no photocatalytic activity under NIR irradiation (see Fig. 6b), the photocatalytic effect of the $NaYF_4$:Yb,Tm@CdS under NIR light should be ascribed to the synergistic influences between $NaYF_4$:Yb,Tm and CdS particles.

Fig. 6b shows the relative concentration C/C_0 *versus* the degradation time of different photocatalysts under Vis-NIR and NIR irradiations, respectively. It can be found that the naked CdS shows good catalytic activity under Vis-NIR irradiation. The degradation ratio of RhB attained to 65% under Vis-NIR irradiation for 75 min. However, it can be also seen from Fig. 6b that the naked CdS has almost no photocatalytic effect under NIR irradiation. This result indicated that the naked CdS possesses good photocatalytic degradation under visible light irradiation. Furthermore, it can be interesting found that the degradation rate of RhB catalyzed by $NaYF_4$:Yb,Tm@CdS composite is obviously faster than that catalyzed by naked CdS under Vis-NIR irradiation. After Vis-NIR light irradiation for 75 min, 82% of RhB is degraded by $NaYF_4$:Yb,Tm@CdS catalyst. In comparison, only 65% of RhB is degraded by naked CdS catalyst. Obviously, these results indicate that the photocatalytic activity of $NaYF_4$:Yb,Tm@CdS is superior to that of naked CdS under Vis-NIR light irradiation. To investigate the stability of the as-prepared samples, we carried out a cyclic photocatalytic

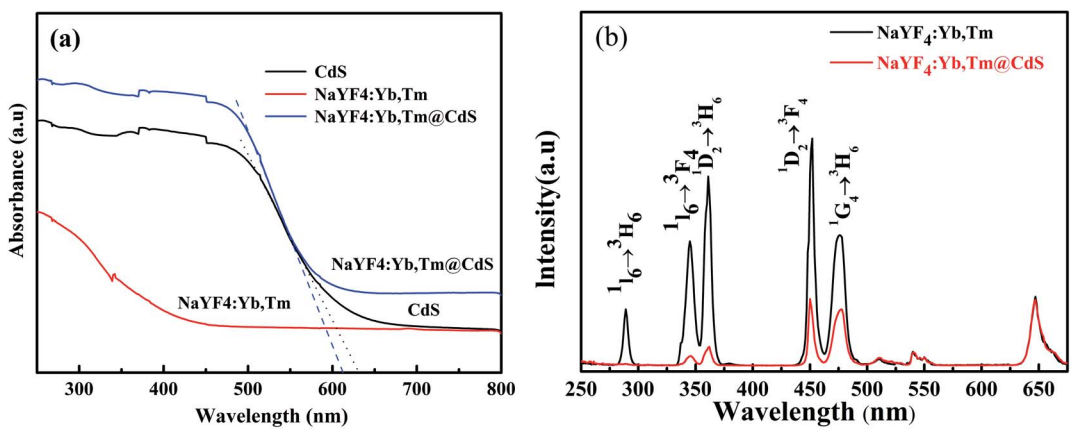

Fig. 5 (a) UV-Vis light absorption spectra of different samples; (b) upconversion photoluminescence (PL) spectra of the NaYF4:Yb,Tm and $NaYF_4$:Yb,Tm@CdS under 980 nm laser excitation at room temperature.

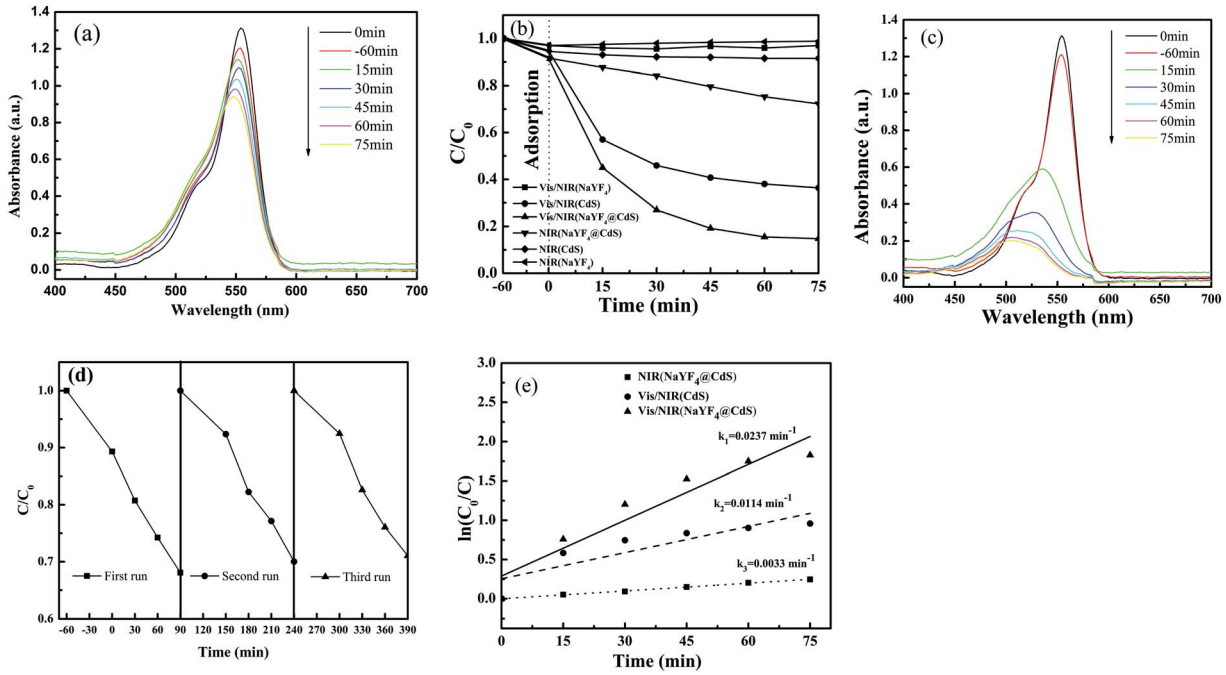

Fig. 6 (a) UV-Vis absorption of the RhB solution catalyzed by $NaYF_4$:Yb,Tm@CdS composite under NIR irradiation; (b) photocatalytic activities of the photocatalysts for the degradation of RhB under different light wavelength band; (c) UV-Vis absorption of the RhB solution catalyzed by $NaYF_4$:Yb,Tm@CdS composite under Vis-NIR irradiation; (d) cycle runs for photocatalytic degradation test using $NaYF_4$:Yb,Tm@CdS as the photocatalyst under NIR irradiation; (e) photocatalytic rate constant of the photocatalysts for the degradation of RhB under different light wavelength band.

degradation test using $NaYF_4$:Yb,Tm@CdS as the photocatalyst. As shown in Fig. 6d, no obvious decrease in the photo-activity of $NaYF_4$:Yb,Tm@CdS can be observed after three consecutive runs, indicating that the $NaYF_4$:Yb,Tm@CdS has good photocatalytic stability.

Most of the photocatalytic reactions follow the Langmuir–Hinshelwood adsorption model, and the L–H model can be simplified to a pseudo-first-order expression: $\ln(C_0/C) = kt$ (where C_0 and C are the equilibrium concentration of adsorption and the concentration of RhB at the irradiation time, t, respectively, and k is apparent rate constant). Using regression-fitting techniques, the linear plots of $\ln(C_0/C)$ *versus* irradiation time t are shown in Fig. 6e. It can be found that the apparent rate constant k for NaYF4:Yb,Tm@CdS (2.37×10^{-2} min^{-1}) is higher than that for naked CdS (1.14×10^{-2} min^{-1}) under Vis-NIR light irradiation, suggesting that the photocatalytic activity of $NaYF_4$:Yb,Tm@CdS is superior to that of naked CdS under Vis-NIR light.

$NaYF_4$:Yb,Tm is an excellent upconversion material and shows typical photoluminescence emission characteristics. Under 980 nm light irradiation, the emission peaks of Tm^{3+} both in UV light region at 290, 347, 362 nm and in visible light region at 452, 476 nm are observed (see Fig. 5b). Fig. 7 shows the enhanced photocatalytic mechanism of $NaYF_4$:Yb,Tm@CdS under Vis-NIR light. Under NIR light irradiation, the Yb^{3+} ions act as sensitizer to absorb the NIR light and transforms NIR light into UV and visible light continuously, then the UV and visible light are absorbed immediately by CdS catalyst on the surface of the $NaYF_4$:Yb,Tm micro-rods to produce electrons and holes in the CB and VB bands, respectively. The electrons and holes can not only directly decompose the RhB in water solution, but also can degrade them indirectly through oxidation of H_2O molecules to ·OH with high oxidative ability.[32,33]

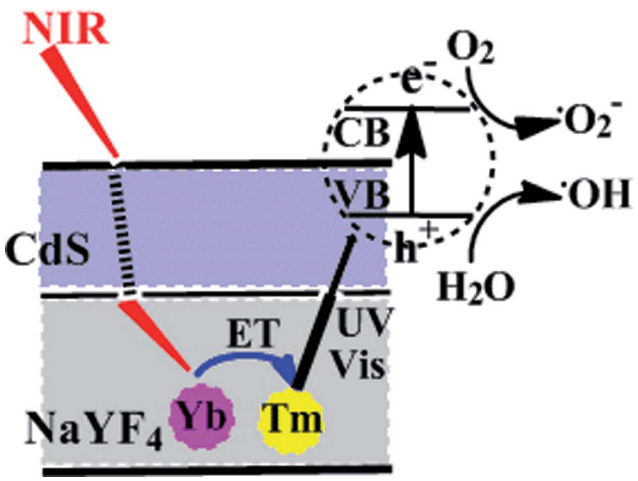

Fig. 7 Illustration of enhanced photocatalytic mechanism of the core–shell $NaYF_4$:Yb,Tm@CdS composite.

4 Conclusions

In summary, hybrid NIR-activated photocatalyst $NaYF_4$:Yb,Tm@CdS core–shell structured composite has been synthesized by hydrothermal method and surface deposition technology. Observation by HRTEM showed that the CdS shell

existed in the form of porous nano-clusters. This microporous-like structure of nano-clusters is beneficial for the catalyst adsorption of the reactant. The photocatalytic experiment verified that the $NaYF_4$:Yb,Tm@CdS micro-rods displayed photocatalytic activity and good photocatalytic stability under NIR light irradiation due to efficient transformation NIR light to UV and visible light by $NaYF_4$:Yb,Tm. Furthermore, the photocatalytic activity of $NaYF_4$:Yb,Tm@CdS is obvious superior to that of naked CdS under Vis-NIR light irradiation.

Conflicts of interest

There are no conflicts to declare.

References

1 X. B. Chen, S. H. Shen, L. J. Guo and S. S. Mao, Semiconductor-based Photocatalytic Hydrogen Generation, *Chem. Rev.*, 2010, **110**(11), 6503–6570.

2 M. Zhou, X. W. Lou and Y. Xie, Two-dimensional nanosheets for photoelectrochemical water splitting: Possibilities and opportunities, *Nano Today*, 2013, **8**(6), 598–618.

3 L. Pan, T. Muhammad, L. Ma, Z. F. Huang, S. Wang, L. Wang, J. J. Zou and X. W. Zhang, MOF-derived C-doped ZnO prepared *via* a two-step calcination for efficient photocatalysis, *Appl. Catal., B*, 2016, **189**, 181–191.

4 G. Q. Shen, L. Pan, Z. Lu, C. Q. Wang, F. Aleem, X. W. Zhang and J. J. Zou, Fe-TiO_2 and Fe_2O_3 quantum dots co-loaded on MCM-41 for removing aqueous rose bengal by combined adsorption/photocatalysis, *Chin. J. Catal.*, 2018, **39**(5), 920–928.

5 R. K. Upadhyay, M. Sharma, D. K. Singh, S. S. Amritphale and N. Chandra, Photodegradation of synthetic dyes using cadmium sulfide nanoparticles synthesized in the presence of different capping agents, *Sep. Purif. Technol.*, 2012, **88**(2), 39–45.

6 J. G. Yu, Y. F. Yu, P. Zhou, W. Xiao and B. Cheng, Morphology-dependent photocatalytic H-2-production activity of CdS, *Appl. Catal., B*, 2014, **156–157**, 184–191.

7 J. Jin, J. G. Yu, G. Liu and P. K. Wong, Single crystal CdS nanowires with high visible-light photocatalytic H-2-production performance, *J. Mater. Chem. A*, 2013, **1**(36), 10927–10934.

8 X. Y. Li, Y. Xi, C. G. Hu and X. Wang, Water induced size and structure phase transition of CdS crystals and their photocatalytic property, *Mater. Res. Bull.*, 2013, **48**(2), 295–299.

9 T. Gao and T. Wang, Two-Dimensional Single Crystal CdS Nanosheets: Synthesis and Properties, *Cryst. Growth Des.*, 2010, **10**(11), 4995–5000.

10 F. Yang, N. N. Yan, S. Huang, Q. Sun, L. Z. Zhang and Y. Yu, Zn-doped CdS nanoarchitectures prepared by hydrothermal synthesis: Mechanism for enhanced photocatalytic activity and stability under visible light, *J. Phys. Chem. C*, 2012, **116**(16), 9078–9084.

11 S. Higashimoto, Y. Nakai, M. Azuma, M. Takahashi and Y. Sakata, One-pot synthesis of imine from benzyl alcohol and nitrobenzene on visible-light responsive CdS-TiO_2 photocatalysts, *RSC Adv.*, 2014, **4**(71), 37662–37668.

12 X. Jia, M. Tahir, L. Pan, Z. F. Huang, X. W. Zhang, L. Wang and J. J. Zou, Direct Z-scheme composite of CdS and oxygen-defected $CdWO_4$: An efficient visible-light-driven photocatalyst for hydrogen evolution, *Appl. Catal., B*, 2016, **198**, 154–161.

13 M. Luo, Y. Liu, J. C. Hu, H. Liu and J. L. Li, One-pot synthesis of CdS and Ni-doped CdS hollow spheres with enhanced photocatalytic activity and durability, *ACS Appl. Mater. Interfaces*, 2012, **4**(3), 1813–1821.

14 R. Levinson, P. Berdahl and H. Akbari, Solar spectral optical properties of pigmentsd-Part I: model for deriving scattering and absorption coefficients from transmittance and reflectance measurements, *Sol. Energy Mater. Sol. Cells*, 2005, **89**(4), 319–349.

15 Y. T. Dong, J. Choi, H. K. Jeong and D. H. Son, Hot Electrons Generated from Doped Quantum Dots *via* Upconversion of Excitons to Hot Charge Carriers for Enhanced Photocatalysis, *J. Am. Chem. Soc.*, 2015, **137**(16), 5549–5554.

16 S. Q. Huang, N. W. Zhu, Z. Y. Lou, L. Gu, C. Miao, H. P. Yuan and A. D. Shan, Near-infrared photocatalysts of $BiVO_4$/CaF_2:Er^{3+}, Tm^{3+}, Yb^{3+} with enhanced upconversion properties, *Nanoscale*, 2014, **6**(3), 1362–1368.

17 Z. Q. Li, C. L. Li, Y. Y. Mei, L. M. Wang, G. H. Du and Y. J. Xiong, Synthesis of rhombic hierarchical YF_3 nanocrystals and their use as upconversion photocatalysts after TiO_2 coating, *Nanoscale*, 2013, **5**(7), 3030–3036.

18 D. X. Xu, Z. W. Lian, M. L. Fu, B. L. Yuan, J. W. Shi and H. J. Cui, Advanced near-infrared-driven photocatalyst: fabrication, characterization, and photocatalytic performance of β-$NaYF_4$:Yb^{3+},Tm^{3+} @ TiO_2 core @ shell microcrystals, *Appl. Catal., B*, 2013, **142–143**, 377–386.

19 G. Y. Shi, Y. F. Mao, G. Z. Ren, L. J. Gong and Z. G. Zhi, Synthesis and photolysis of $NaYF_4$@SiO_2@TiO_2 core–shell nanocomposites, *Opt. Commun.*, 2014, **332**(4), 219–222.

20 X. Y. Guo, W. Y. Song, C. F. Chen, W. H. Di and W. P. Qin, Near-infrared photocatalysis of β-$NaYF_4$:Yb^{3+},Tm^{3+}@ZnO composites, *Phys. Chem. Chem. Phys.*, 2013, **15**(35), 14681–14688.

21 M. J. Tou, Z. G. Luo, S. Bai, F. Y. Liu, Q. X. Chai, S. Li and Z. Q. Li, Sequential coating upconversion NaYF4:Yb,Tm nanocrystals with SiO2 and ZnO layers for NIR-driven photocatalytic and antibacterial applications, *Mater. Sci. Eng., C*, 2017, **70**(s1), 1141–1148.

22 C. H. Li, F. Wang, J. A. Zhu and J. C. Yu, NaYF4 Yb,Tm/CdS composite as a novel near-infrared-driven photocatalyst, *Appl. Catal., B*, 2010, **100**(3), 433–439.

23 F. Wang, Y. Han, C. S. Lim, Y. H. Lu, J. Wang, J. Xu, H. Y. Chen, C. Zhang, M. H. Hong and X. G. Liu, Simultaneous phase and size control of upconversion nanocrystals through lanthanide doping, *Nature*, 2010, **463**(7284), 1061–1065.

24 N. Bogdan, F. Vetrone, G. A. Ozin and J. A. Capobianco, Synthesis of Ligand-Free Colloidally Stable Water Dispersible Brightly Luminescent Lanthanide-Doped

Upconverting Nanoparticles, *Nano Lett.*, 2011, **11**(2), 835–840.

25 S. W. Duo, J. J. Zhang, H. Zhang, Z. Chen, C. P. Zhong and T. Z. Liu, Synthesis of NaYF4:Yb^{3+},Tm^{3+} @ TiO_2 and $NaYF_4$:Yb^{3+},Tm^{3+} @TiO_2 @ Au nanocomposites and effective upconversion-driven photocatalytic properties, *Opt. Mater.*, 2016, **62**, 240–249.

26 Y. N. Tang, W. H. Di, X. S. Zhai, R. Y. Yang and W. P. Qin, NIR-responsive photocatalytic activity and mechanism of $NaYF_4$:Yb,Tm@TiO_2 core-shell nanoparticles, *ACS Catal.*, 2013, **3**(3), 405–412.

27 W. K. Su, M. M. Zheng, L. Li, K. Wang, R. Qiao, Y. J. Zhong, Y. Hua and Z. Q. Li, Directly coat TiO_2 on hydrophobic $NaYF_4$:Yb,Tm nanoplates and regulate their photocatalytic activities with the core size, *J. Mater. Chem. A*, 2014, **2**(33), 13486–13491.

28 J. J. Li, Y. A. Wang, W. Z. Guo, J. C. Keay, T. D. Mishima, M. B. Johnson and X. G. Peng, Large-scale synthesis of nearly monodisperse CdSe/CdS core/shell nanocrystals using air-stable reagents *via* successive ion layer adsorption and reaction, *J. Am. Chem. Soc.*, 2003, **125**(41), 12567–12575.

29 M. J. Tou, Y. Y. Mei, S. Bai, Z. G. Luo, Y. Zhang and Z. Q. Li, Depositing CdS nanoclusters on carbon-modified $NaYF_4$:Yb,Tm upconversion nanocrystals for NIR-light enhanced photocatalysis, *Nanoscale*, 2015, **8**(1), 553–562.

30 S. Y. Tan, P. P. Yang, N. Niu, S. L. Gai, J. Wang, X. Y. Jing and J. Lin, Monodisperse and core-shell structured $NaYF_4$:Ln@SiO_2 (Ln=Yb/Er, Yb/Tm) microspheres: Synthesis and characterization, *J. Alloys Compd.*, 2010, **490**(1), 684–689.

31 W. Wang, M. Y. Ding, C. H. Lu, Y. R. Ni and Z. Z. Xu, A study on upconversion UV-vis-NIR responsive photocatalytic activity and mechanisms of hexagonal phase $NaYF_4$:Yb^{3+},Tm^{3+}@TiO_2 core-shell structured photocatalyst, *Appl. Catal., B*, 2014, **144**(1), 379–385.

32 J. Wang, T. Ma, G. Zhang, Z. H. Zhang, X. D. Zhang, Y. F. Jiang, G. Zhao and P. Zhang, Preparation of novel nanometer TiO_2 catalyst doped with upconversion luminescence agent and investigation on degradation of acid red B dye using visible light, *Catal. Commun.*, 2007, **8**(3), 607–611.

33 L. Pan, G. Q. Shen, J. W. Zhang, X. C. Wei, L. Wang, J. J. Wang, J. J. Zou and X. W. Zhang, TO2-ZnO composite sphere decorated with ZnO clusters for effective charge isolation in photocatalysis, *Ind. Eng. Chem. Res.*, 2015, **54**(29), 7226–7232.